Centrum voor Wiskunde en Informatica
Centre for Mathematics and Computer Science

B. Koren

Evaluation of second order schemes and defect correction
for the multigrid computation of airfoil flows
with the steady Euler equations

Department of Numerical Mathematics Report NM-R8616 June

The Centre for Mathematics and Computer Science is a research institute of the Stichting Mathematisch Centrum, which was founded on February 11, 1946, as a nonprofit institution aiming at the promotion of mathematics, computer science, and their applications. It is sponsored by the Dutch Government through the Netherlands Organization for the Advancement of Pure Research (Z.W.O.).

Evaluation of Second Order Schemes and Defect Correction for the Multigrid Computation of Airfoil Flows with the Steady Euler Equations

Barry Koren
Centre for Mathematics and Computer Science
P.O. Box 4079, 1009 AB Amsterdam, The Netherlands

Second order accurate Euler flow solutions are presented for some standard airfoil test cases. Second order accuracy is obtained by a defect correction process. Several schemes are considered for the computation of the second order defect. In each defect correction cycle, the solution is computed by a non-linear multigrid iteration, in which Collective Symmetric Gauss-Seidel relaxation is used as smoothing procedure. A finite volume Osher discretization is applied. The computational method does not require tuning of parameters. The solutions obtained show a good resolution of all flow phenomena, and are obtained at low computational costs. The rate of convergence is grid-independent. The method contributes to the state of the art in efficiently computing airfoil flows with discontinuities.

1980 Mathematics Subject Classification: 65N30, 76G15, 76H05.
Key Words and Phrases: steady Euler equations, second order schemes, defect correction, multigrid methods.
Note: This report will be submitted for publication elsewhere.

1. Introduction

Recently, a very efficient multigrid method has been developed for the solution of a robust, first order accurate discretization of the Euler equations [7]. Two well-known drawbacks of first order accurate discretizations of the Euler equations are: (i) their need for relatively fine grids in smooth flow regions, and (ii) their strong smearing of discontinuities that are not aligned with the grid. Second order discretizations yield a strong improvement of both drawbacks. However, second order discretizations are not solved with the same efficiency by the multigrid method developed. Further, with second order discretizations stability problems easily arise and spurious non-monotonicity (wiggles) may be introduced. Motivated by the requirement of computational efficiency, Hemker [6] and Spekreijse [12] investigated a solution method for stable, but apart from that, arbitrary second order schemes. The method is based on the defect correction principle [3].

In this paper, we show that these techniques are also feasible for the efficient computation of flows around airfoils. For five second order schemes, we compare the solution by a defect correction process. The discussion is restricted to a number of well-known benchmark problems from [11] and [14]: the NACA0012-airfoil at $M_\infty = 0.63$, $\alpha = 2°$; $M_\infty = 0.8$, $\alpha = 1.25°$; $M_\infty = 0.85$, $\alpha = 1°$ and $M_\infty = 1.2$, $\alpha = 7°$, and the NLR7301-airfoil at $M_\infty = 0.721$, $\alpha = -0.194°$ (design conditions).

In section 2, we briefly describe the basic discretization technique. In section 3, we discuss the solution method used: non-linear multigrid as an inner iteration for the solution of the elementary first order system and defect correction as an outer iteration for the solution of the second order system. In section 4, we describe the five second order schemes that were used and compared in our computations. The main results of this paper are given in section 5. Conclusions are summarized in section 6.

Report NM-R8616
Centre for Mathematics and Computer Science
P.O. Box 4079, 1009 AB Amsterdam, The Netherlands

2. Discretization

The steady 2-D Euler equations can be written on the domain Ω as

$$\frac{\partial f(q)}{\partial x} + \frac{\partial g(q)}{\partial y} = 0, \text{ with} \tag{2.1}$$

$$q = \begin{bmatrix} \rho \\ \rho u \\ \rho v \\ \rho e \end{bmatrix}, f = \begin{bmatrix} \rho u \\ \rho u^2 + p \\ \rho uv \\ \rho u(e + \frac{p}{\rho}) \end{bmatrix}, g = \begin{bmatrix} \rho v \\ \rho vu \\ \rho v^2 + p \\ \rho v(e + \frac{p}{\rho}) \end{bmatrix}, \text{ and} \tag{2.2}$$

$$e = \frac{1}{\gamma - 1}\frac{p}{\rho} + \frac{1}{2}(u^2 + v^2). \tag{2.3}$$

Here, ρ, u, v, p and γ denote respectively: density, velocity components in x- and y-direction, static pressure and ratio of specific heats.

Following [7], we solve the Euler equations in their integral form

$$\int_{\delta\Omega^*} (f n_x + g n_y) ds = 0. \tag{2.4}$$

With $\delta\Omega^*$ we denote the boundary of an arbitrary subregion $\Omega^* \subset \Omega$, and with n_x and n_y the components of the outward normal with unit length, along $\delta\Omega$. A simple way to discretize (2.4) is to subdivide Ω into disjoint quadrilateral subregions Ω_{ij} (finite volumes), and to assume that the flux functions f and g are constant along each volume wall. This gives us the following discretization:

$$\sum_{k=1}^{4} \{ f(q^l_{ij,k}, q^r_{ij,k}) n_{x_{ij,k}} + g(q^l_{ij,k}, q^r_{ij,k}) n_{y_{ij,k}} \} s_{ij,k} = 0, \text{ for all } ij, \tag{2.5}$$

in which the subscript k refers to the kth wall of the quadrilateral volume Ω_{ij}, and the superscripts l and r to the left and right side of this wall respectively.

For the Euler equations, because of their rotational invariance, (2.5) may be further simplified to

$$\sum_{k=1}^{4} \{ T^{-1}_{ij,k} f(T_{ij,k} q^l_{ij,k}, T_{ij,k} q^r_{ij,k}) s_{ij,k} = 0, \text{ for all } ij, \text{ with} \tag{2.6}$$

$$T_{ij,k} = \begin{bmatrix} 1 & 0 & 0 & 0 \\ 0 & n_{x_{ij,k}} & n_{y_{ij,k}} & 0 \\ 0 & -n_{y_{ij,k}} & n_{x_{ij,k}} & 0 \\ 0 & 0 & 0 & 1 \end{bmatrix}. \tag{2.7}$$

In each volume, we assume the state to be an approximation of the mean value of the exact solution. When we take $q^l_{ij,k}$ and $q^r_{ij,k}$ equal to the states in volume Ω_{ij} and its neighbouring volume $\Omega_{ij,k}$, (2.6) is first order accurate only. Second order accuracy can be obtained in a simple way by determining $q^l_{ij,k}$ and $q^r_{ij,k}$ as either interpolations or extrapolations by low degree piecewise polynomial functions, using two or three adjacent volume states. Schemes for inter- and extrapolation of volume states are called projection schemes [9].

For the evaluation of the flux vector f at the volume walls, we consider the flow at each volume wall as the local solution of the 1-D Riemann problem for the two gas states $q^l_{ij,k}$ and $q^r_{ij,k}$. For the solution of the 1-D Riemann problem, we have chosen the approximate Riemann solver as proposed by Osher [10]. The choice for Osher's scheme is motivated among others by: (i) its consistent treatment of boundary conditions, and particularly (ii) its suitability for Newton-type solution techniques.

3. Solution method

When one uses the first order discretization, the non-linear system (2.6) becomes

$$\sum_{k=1}^{4} T_{ij,k}^{-1} f(T_{ij,k} q_{ij}, T_{ij,k} q_{ij,k}) s_{ij,k} = 0, \text{ for all } ij, \tag{3.1}$$

in which $q_{ij,k}$ denotes the state in $\Omega_{ij,k}$.

To solve this system, we considered point (=volume) relaxation methods, in which we used one or more local Newton steps for the collective relaxation of the 4 unknowns in each single volume. The most efficient relaxation was obtained by selecting a large tolerance for the Newton iteration, so that in all but exceptional cases only a single Newton step was taken. These relaxation methods are simple and robust, but need an acceleration. When one uses, as in [7] and [8], Collective Symmetric Gauss-Seidel as a point relaxation method, a suitable acceleration technique is found in multigrid. As a very efficient and robust multigrid technique we use: the full approximation scheme (FAS), preceded by full multigrid (FMG) to obtain a good initial estimate [5].

However, when one uses a higher order discretization and adopts this solution method, one will lose in efficiency. Point Gauss-Seidel will no longer be a good smoother. To circumvent the difficulty of finding a sufficiently good smoother, we use a defect correction process (DCP) as solution method [3]. Denoting the system of equations resulting from a first and second order discretization as $N_h^1(q_h)=0$ and $N_h^2(q_h)=0$ respectively, DCP can be written as

$$N_h^1(q_h^1) = 0, \tag{3.2a}$$

$$N_h^1(q_h^{n+1}) = N_h^1(q_h^n) - N_h^2(q_h^n), \quad n = 1,2,... \tag{3.2b}$$

As solution method for $N_h^1(q_h)=r_h$ as it appears in both (3.2a) and (3.2b), we maintain the efficient multigrid method just described.

Although the second order discretization only manifests itself via the righthand side, the efficiency of this indirect solution method is amazingly good. For sufficiently smooth problems, both theory [5] and practice [6] show that already q_h^2, the first iterand in (3.2b), is second order accurate.

4. Projection schemes

As standard projection schemes, we consider the central, the upwind and an upwind biased scheme. These three schemes can be written as

$$q^l_{i+\frac{1}{2},j} = q_{i,j} + \frac{1+\kappa}{4}(q_{i+1,j} - q_{i,j}) + \frac{1-\kappa}{4}(q_{i,j} - q_{i-1,j}), \text{ and} \tag{4.1a}$$

$$q^r_{i+\frac{1}{2},j} = q_{i+1,j} + \frac{1+\kappa}{4}(q_{i,j} - q_{i+1,j}) + \frac{1-\kappa}{4}(q_{i+1,j} - q_{i+2,j}), \tag{4.1b}$$

in which $i+\frac{1}{2}$ denotes the wall separating volume i and $i+1$. For $\kappa=1, \kappa=-1$ and $\kappa=\frac{1}{3}$, we get the central, the upwind and the upwind biased scheme respectively. Similar relations hold for $q^l_{i,j+\frac{1}{2}}$ and $q^r_{i,j+\frac{1}{2}}$. A property of the central scheme is that it makes the Riemann solver superfluous. Properties of all three schemes are: (i) that they cannot be applied in a consistent way in the neighbourhood of boundaries, and (ii) that they may yield solutions with wiggles.

As a projection scheme which is consistent near boundaries, Hemker [6] introduced the so-called superbox scheme. A superbox is defined as a set of 2×2 volumes. At the 4 inner walls of a superbox the simple central projection scheme is used, whereas at the 8 outer walls the upwind scheme is used. A property of the superbox scheme is that its solutions are second order accurate per arbitrary set of 2×2 volumes, but not per single volume. The remaining lower order error contains only high frequencies. This error can be eliminated in a simple way by computing states at volume vertices as averages over neighbouring volumes. (Formal proofs can be given.) Similar to the above-mentioned schemes, the superbox scheme may also yield solutions with wiggles.

Projection schemes exist which, by the use of flux limiters, can yield solutions without spurious non-monotonicity. Examples are the schemes proposed by van Leer and van Albada [1]. These schemes can be written as

$$q^l_{i+\frac{1}{2},j} = q_{i,j} + \frac{1}{2}\psi(R_{i,j})(q_{i,j} - q_{i-1,j}), \tag{4.2a}$$

$$q^r_{1+\frac{1}{2},j} = q_{i+1,j} + \frac{1}{2}\psi(\frac{1}{R_{i+1,j}})(q_{i+1,j} - q_{i+2,j}), \tag{4.2b}$$

with ψ denoting the flux limiter, and with

$$R_{i,j} = \frac{q_{i+1,j} - q_{i,j}}{q_{i,j} - q_{i-1,j}}. \tag{4.3}$$

The van Leer limiter is defined by

$$\psi(R) = \frac{R + |R|}{R + 1}, \tag{4.4}$$

and the van Albada limiter by

$$\psi(R) = \frac{R^2 + R}{R^2 + 1}. \tag{4.5}$$

A general analysis of flux limiters can be found in [13]. Projection schemes using flux limiters need (at least) three volume states per projection. This implies that the superbox scheme cannot be made monotone by this technique.

Both the van Leer and the van Albada scheme cannot be used in a consistent way near boundaries. Near boundaries one has to use other schemes, as for instance the central and the upwind scheme, which may both introduce some small wiggles.

We prefer the van Albada scheme, because at the upstream side of shock waves ($R \gg 1$), it is close to the upwind scheme, which is a natural scheme in those regions.

5. Results

For all results presented, we used O-type grids with the outer boundary at an approximate distance from the airfoil of either 25 or 100 chord lengths. For both distances, we imposed the unperturbed flow at the outer boundary, although we did not overimpose. (I.e. for e.g. a subsonic outer boundary, we did not impose more than 3 boundary conditions at the inlet part of that boundary and not more than 1 boundary condition at the outlet part.)

For each of the projection schemes considered, the Kutta condition was automatically satisfied for all flows. For all flows a streamline smoothly left the trailing edge. An explanation for the fact that there is no flow around the airfoil's tail may be the property of all discretizations that they are non-isentropic. Along both the upper and lower airfoil surface, they all generate spurious changes of total pressure. As a consequence, a flow around the airfoil's tail would in general result in a stagnation at two different pressures, which is an unstable flow situation.

At first, we investigated the iterative solution method for the non-linear systems (3.2a) and (3.2b). It was found that the convergence rate is independent of the starting point of the relaxation sweeps. However, we found that for efficient smoothing one should always make symmetric sweeps. So, for instance if one starts at the airfoil, one should not stop at the outer boundary, but return from the outer boundary to the airfoil and stop there.

Concerning the multigrid strategy, it appeared that the straightforward use of V-cycles with a single symmetric pre- and post-relaxation per level gives a very good convergence rate. For all results presented in this paper, we used a coarsest grid with 8 volumes tangentially to the airfoil and either 4 or 2 volumes radially. We notice that this is extremely coarse, if seen in the light of suspicions raised

by ERIKSSON & RIZZI [4] against the possibilities of a multigrid method.

For the evaluation of the various projection schemes in combination with DCP, we considered a standard test case for the airfoil NACA0012, namely the transonic flow with shock, occuring at $M_\infty = 0.8$ and $\alpha = 1.25°$.

First, to investigate the convergence properties of DCP for the various projection schemes, we performed for each scheme 10 DCP-cycles, with 5 FAS-cycles per DCP-cycle. As finest grid, we used a moderately stretched 32×16-grid (fig. 5.1), yielding a 3-level multigrid strategy.

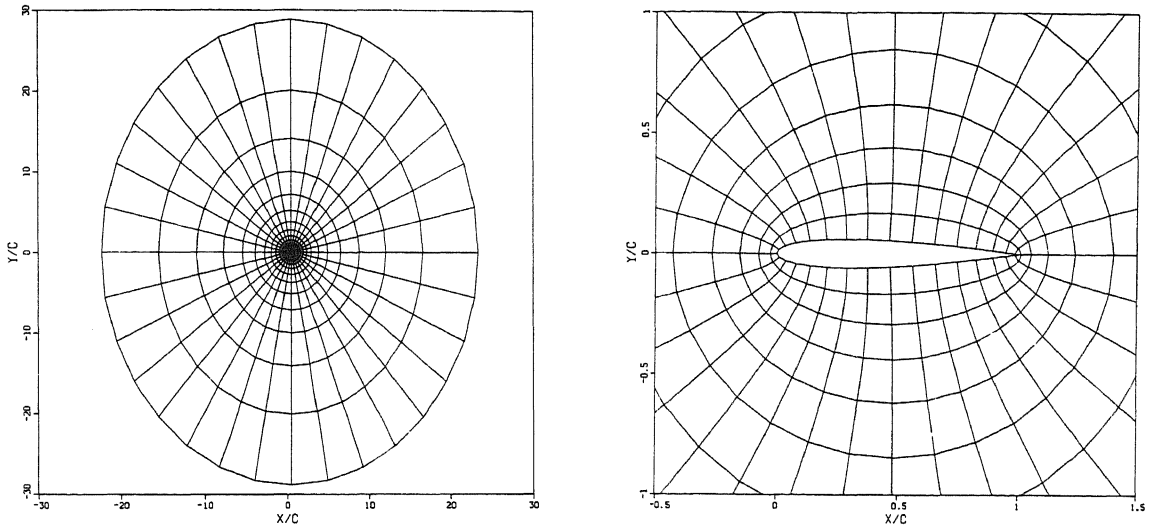

a. In full.

b. In detail.

Fig. 5.1 : 32×16-grid, NACA0012-airfoil.

In fig. 5.2a, convergence histories are given by graphs of the residual ratio $\sum_{i=1}^{4} |\overline{r}_h^n(i)| / \sum_{i=1}^{4} |\overline{r}_h^1(i)|$ versus the number of FAS-cycles. Here, $\overline{r}_h^n$ denotes the summation over all volumes of $r_h^n = N_h^2(q_h^n)$, i the ith residual component, and n the nth iterand in (3.2). As starting point in the convergence histories, the first order solution obtained from (3.2a) is used. The vertical lines mark the beginnings and ends of the DCP-cycles. In fig. 5.2b, graphs are given of the surface distribution of the entropy ratio s/s_∞, with $s = p\rho^{-\gamma}$. For this, the curves with circular markers indicate the upper surface distributions, whereas the curves with triangular markers indicate the lower surface distributions. Except for the superbox scheme, the markers correspond with the x-locations of the volume wall centres at the airfoil's surface. For the superbox scheme, due to the averaging, they correspond with the volume wall vertices at the airfoil's surface.

It appears that both the central and upwind scheme lead to divergence of DCP. For the central scheme, the shock behaves as source of instability. For the upwind scheme, the stagnation region behaves as such. Recently, Hemker [private communication] explained the instability of DCP for the upwind scheme by applying Local Mode Analysis to the linear convection equation.

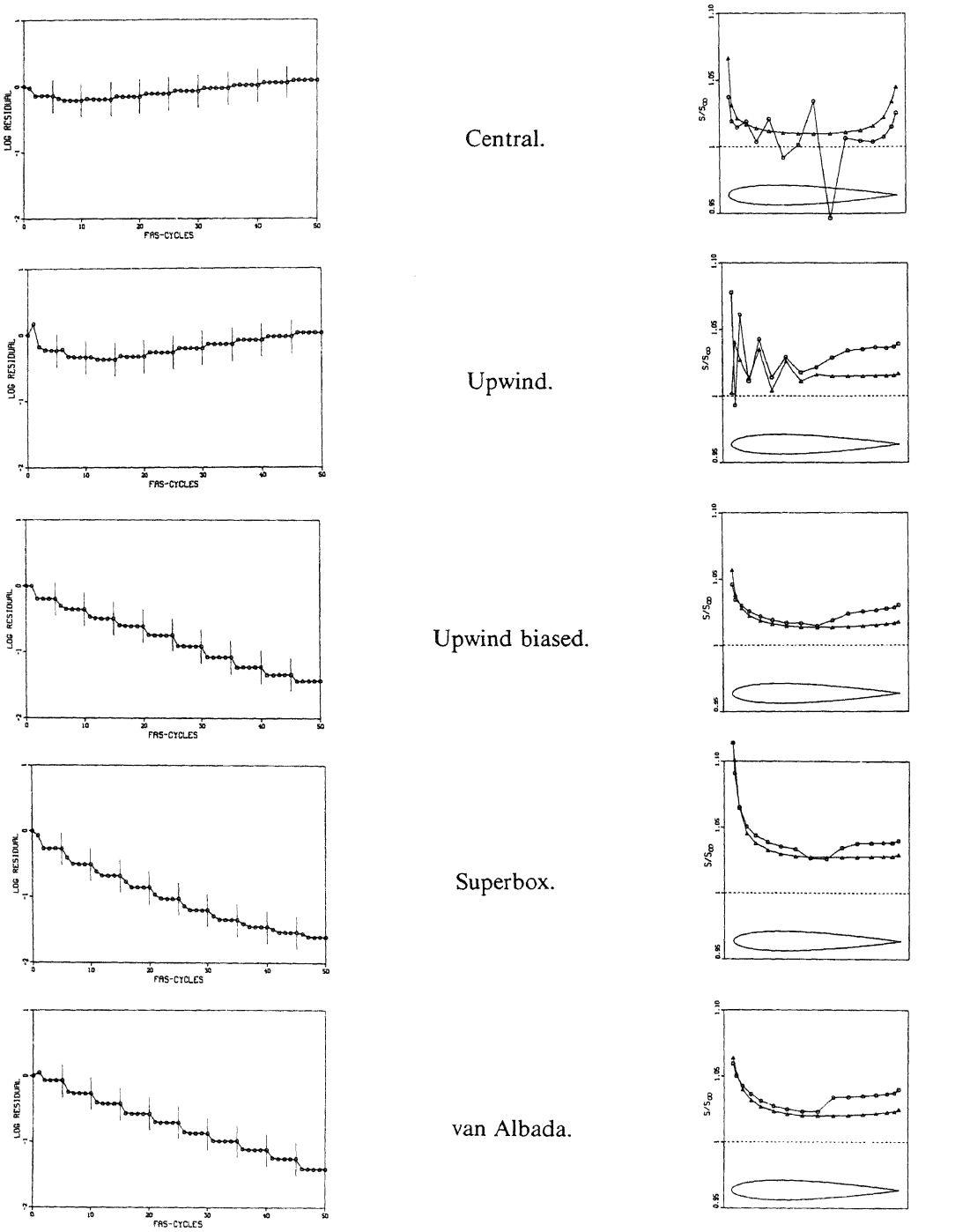

a. Convergence histories. b. Surface entropy distributions.

Fig. 5.2 : Results second order schemes (NACA0012, $M_\infty = 0.8$, $\alpha = 1.25°$).

The convergence histories of fig. 5.2a suggest that the use of 1 or 2 FAS-cycles per DCP-cycle is sufficient, irrespective of the projection scheme used. To investigate the optimal number of FAS-cycles per DCP-cycle, we performed successively: 20 DCP-cycles with 1 FAS-cycle per DCP-cycle, and 10 DCP-cycles with 2 FAS-cycles per DCP-cycle. As finest grid, we used again the 32×16-grid as shown in fig. 5.1.

The convergence histories obtained are given in fig. 5.3. As starting point, we used again the first order solution obtained from (3.2a). It clearly appears from fig. 5.3 that the strategy with 1 FAS-cycle per DCP-cycle is most efficient for each of the three projection schemes considered.

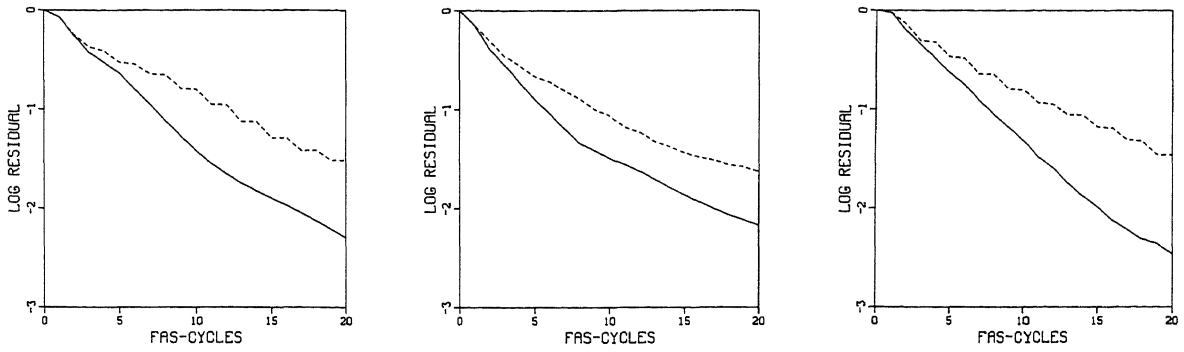

a. Upwind biased. b. Superbox. c. van Albada.

Fig. 5.3: Convergence histories for 1 FAS-cycle per DCP-cycle (solid) and 2 FAS-cycles per DCP-cycle (dashed), (NACA0012, $M_\infty = 0.8$, $\alpha = 1.25°$).

Next, we compared some qualitative properties of the converged solutions of the first order, upwind biased, superbox and van Albada scheme. As finest grid, we used again the 32×16-grid. To be sure that the solutions were converged, we used: 10 FAS-cycles for the first order scheme, and 50 DCP-cycles with 1 FAS-cycle per DCP-cycle for the three second order schemes.

The pressure distributions obtained are given in fig. 5.4. In each graph, the upper dashed line indicates the critical pressure, and the lower the stagnation pressure. The meaning of the markers is the same as in fig. 5.2b. Clearly visible in fig. 5.4 is the strong under- and overshoot at the shock wave, as obtained with the upwind biased and superbox scheme. The small wiggles upstream of the shock, generated by the van Albada scheme must be due to the central and upwind projection that were used near boundaries. Compared with the first order scheme, all three second order schemes give an improvement of the stagnation pressure.

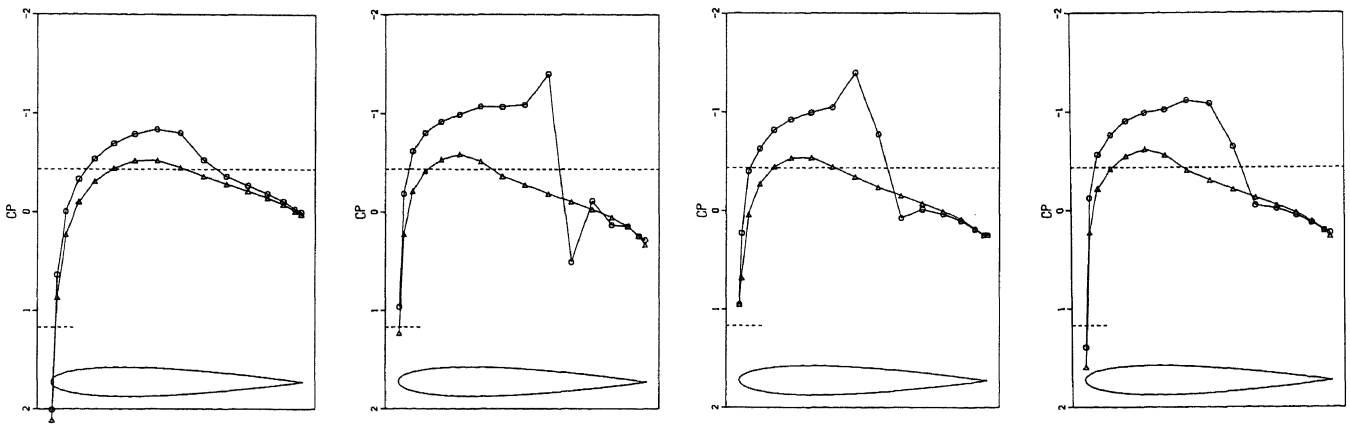

a. First order. b. Upwind biased. c. Superbox. d. van Albada.

Fig. 5.4 : Converged surface pressure distributions (NACA0012, $M_\infty = 0.8$, $\alpha = 1.25°$).

When we take monotonicity at full convergence as an absolute requirement to be fulfilled, only the first order and van Albada scheme can be used. However, since only a few DCP-cycles are necessary (and desired of course), the question arises how spurious non-monotonicity at a shock develops in the first DCP-cycles. To investigate this, we recomputed the transonic flow with shock for the first order scheme, and for the three second order schemes for which DCP converges. As finest grid, we now

used a similar, but four times finer grid; a 128×64-grid (fig. 5.5). As DCP-strategy, we used 10 DCP-cycles with 1 FAS-cycle per DCP-cycle.

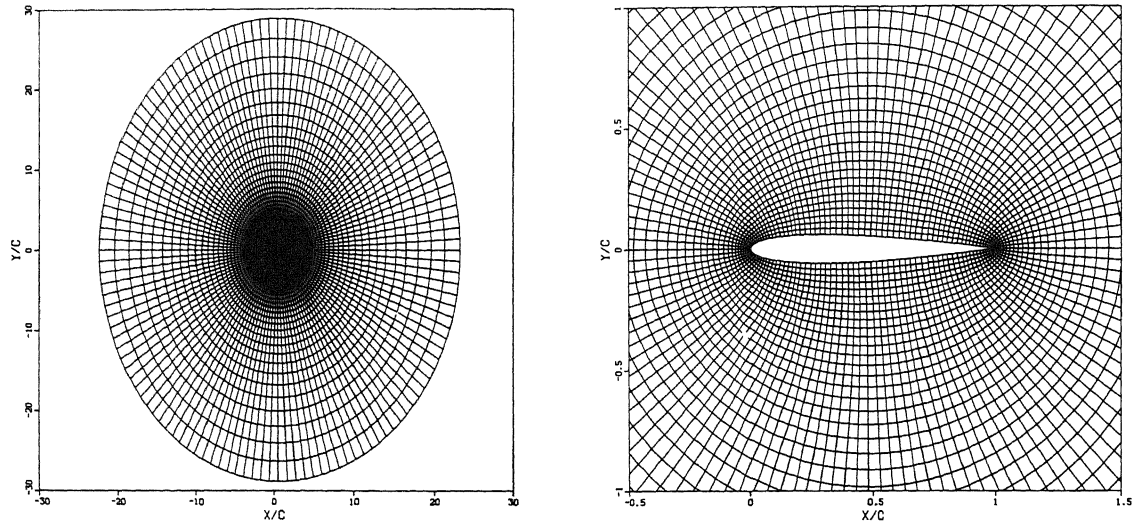

a. In full. b. In detail.

Fig. 5.5 : 128×64-grid, NACA0012-airfoil.

The results obtained are given in fig. 5.6-5.8. Fig. 5.6a and 5.6b show the first order pressure distribution, as obtained after 1 and 10 FAS-cycles respectively. The first pressure distribution (fig. 5.6a) is that of the first order solution obtained from (3.2a). The second one (fig. 5.6b) is that of the fully converged first order solution. The meaning of the markers and dashed lines in the graphs is the same as before. Fig. 5.7 shows for the three second order schemes the pressure distribution, as obtained after successively the 1st, 2nd, 3rd and 10th DCP-cycle. Fig. 5.8 shows surface entropy distributions.

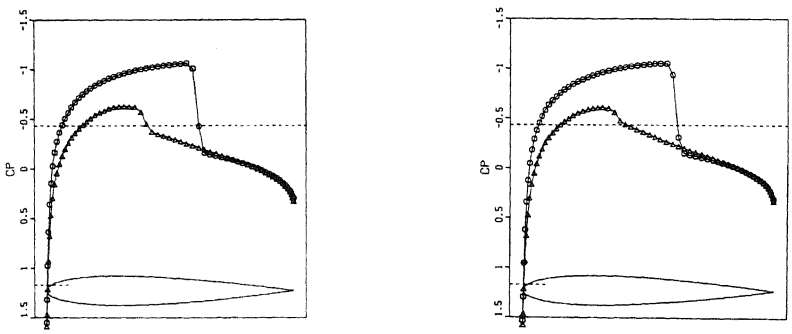

a. After 1 FAS-cycle. b. After 10 FAS-cycles.

Fig. 5.6 : First order surface pressure distributions (NACA0012, $M_\infty = 0.8$, $\alpha = 1.25°$).

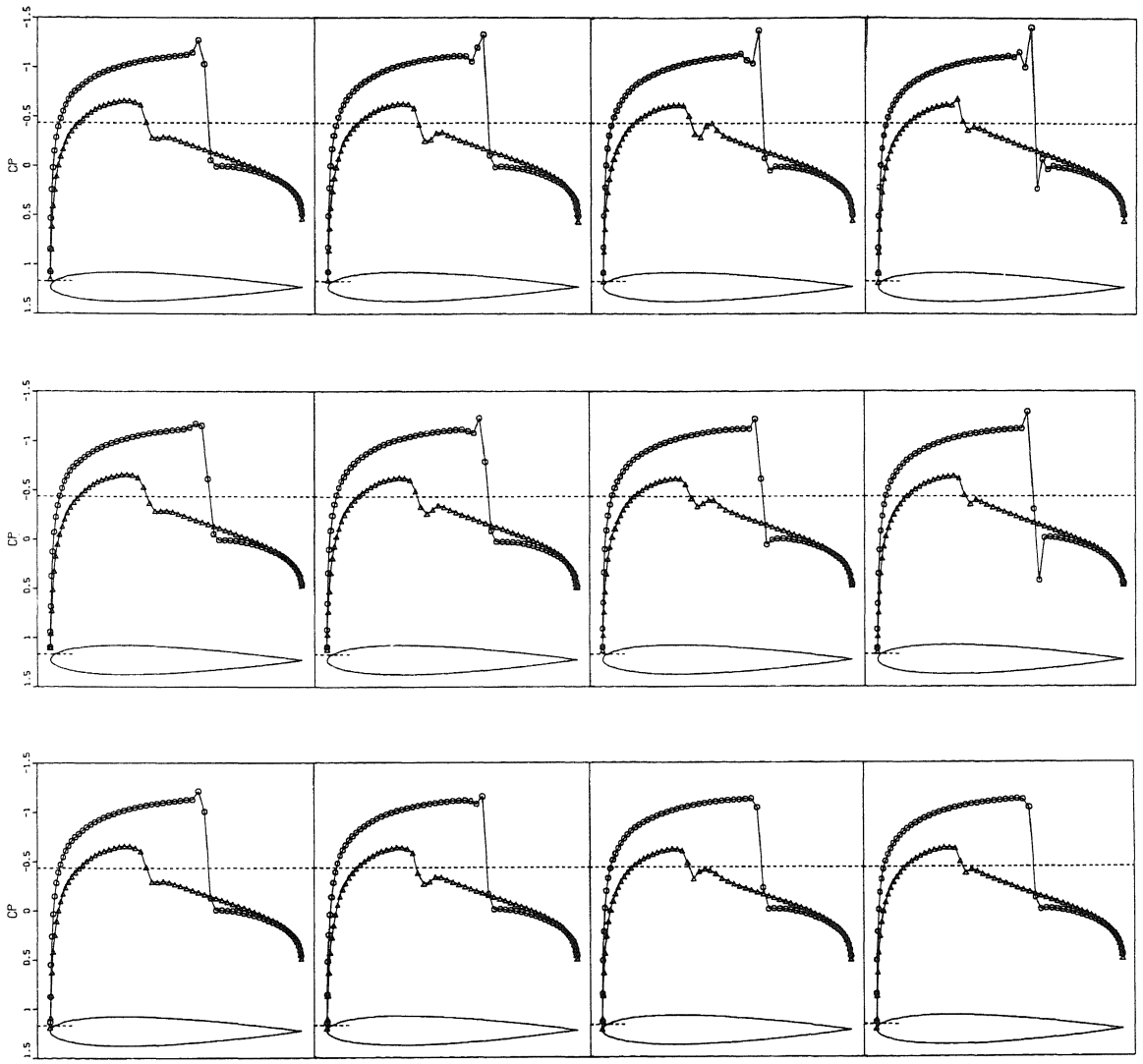

a. Upwind biased.

b. Superbox.

c. van Albada.

After 1st DCP-cycle. After 2nd DCP-cycle. After 3rd DCP-cycle. After 10th DCP-cycle.

Fig. 5.7: Convergence histories surface pressure distribution second order schemes (NACA0012, $M_\infty = 0.8$, $\alpha = 1.25°$).

From fig 5.7, an opposite behaviour after the 1st DCP-cycle becomes clear. The small wiggles, as obtained with all three schemes after the 1st DCP-cycle, grow in the following DCP-cycles for the upwind biased and superbox scheme, but shrink for the van Albada scheme. The van Albada scheme yields a nearly wiggle-free solution after the 3rd DCP-cycle. Remarkable for all three schemes is the excellent improvement of the stagnation pressure which is obtained in the 1st DCP-cycle (fig. 5.6a and 5.7).

In fig. 5.8, all three second order schemes show an excellent improvement of the entropy distribution. The upwind biased scheme shows the best improvement.

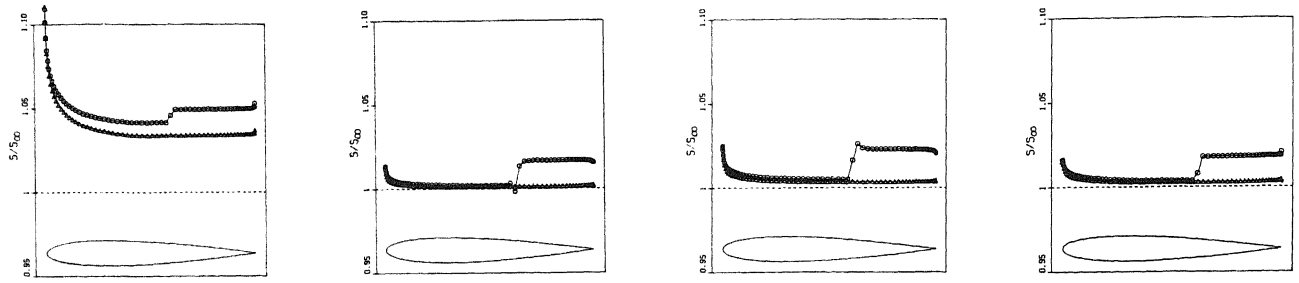

a. First order. b. Upwind biased. c. Superbox. d. van Albada.

Fig. 5.8 : Surface entropy distributions after 10th FAS-cycle (first order scheme) and 10th DCP-cycle (second order schemes), (NACA0012, $M_\infty = 0.8$, $\alpha = 1.25°$).

In fig. 5.9, we make a comparison with computational results obtained by other investigators, for the transonic flow with shock. In fig. 5.9a, the left graph shows the pressure distributions that we obtained after 10 DCP-cycles, whereas the right graph stems from [11]. In fig. 5.9b, we did the same with as reference a graph from [14].

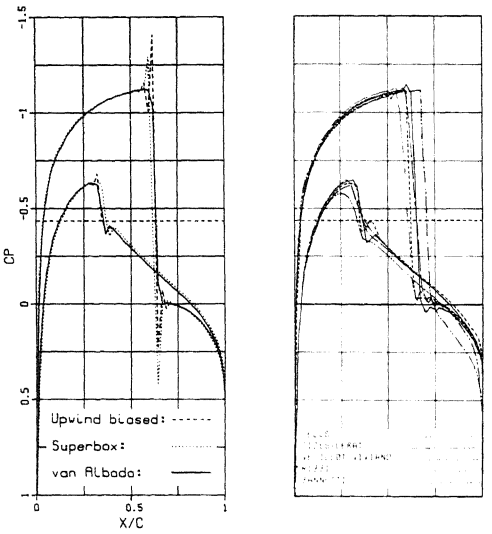

a. Surface pressure distributions; present results (left) and reference results (right).

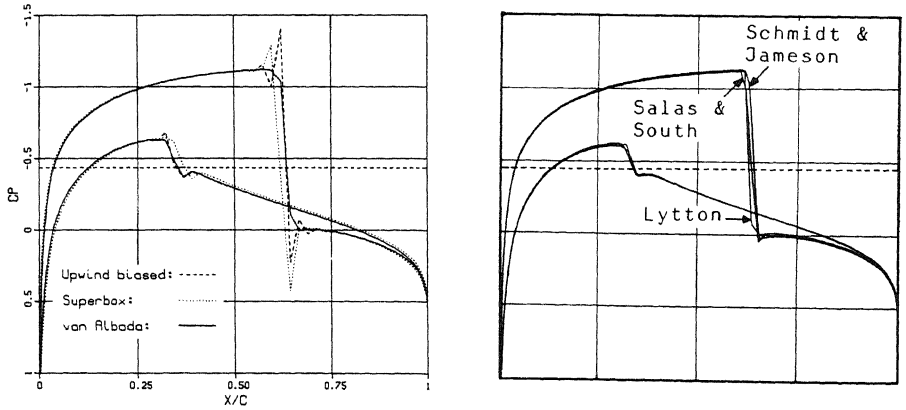

b. Surface pressure distributions; present results (left) and reference results (right).

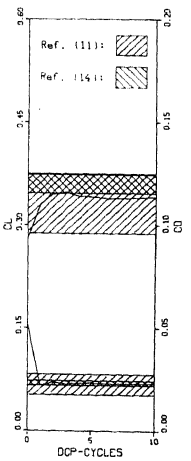

c. Convergence history lift and drag coefficient (van Albada scheme).

Fig. 5.9: Results for NACA0012-airfoil at $M_\infty = 0.8$ and $\alpha = 1.25°$.

In fig. 5.9a, the agreement between the various reference results is poor. This is partly caused by wiggles, but mostly by a large scattering in shock position. This scattering is smaller in the more recent reference results of fig. 5.9b. The agreement between our results and these reference results is good. However, the under- and overshoots, as generated by the upwind biased and superbox scheme, are more severe than those of any of the reference results.

In fig. 5.9c, we present for the van Albada scheme the convergence history of the lift and drag coefficient. As starting point, we took again the solution obtained from (3.2a). The lift and drag as computed by the other investigators are spread over the shaded areas. One shading represents all (5) Euler results from [11], the other shading all (7) Euler results from [14].

In the first DCP-cycle, the lift always shows an increase, whereas the drag always shows a decrease. Clearly visible in fig. 5.9c, is the excellent improvement of the drag, which is obtained in the first DCP-cycle. (Main cause of this is the strong improvement of the stagnation pressure in the first DCP-cycle.) When we take the results from [11] as a standard, we see that we need 1 DCP-cycle. With the results from [14] as a standard, we find a lift which is slightly too low. The cause of this discrepancy is thought to be the fact that the outer boundary is not far enough ($\sim$ 25 chord lengths) from the airfoil. We generated a new fine grid (fig. 5.10), with a twice smaller number of volumes in radial direction (32 instead of 64), but yet with an outer boundary at $\sim$ 100 chord lengths, and a twice smaller volume height at the airfoil! Results of a computation with this new grid are given in fig. 5.11. The improvements are evident. (Concerning the entropy error (fig. 5.11a), an arbitrary good improvement seems to be possible.)

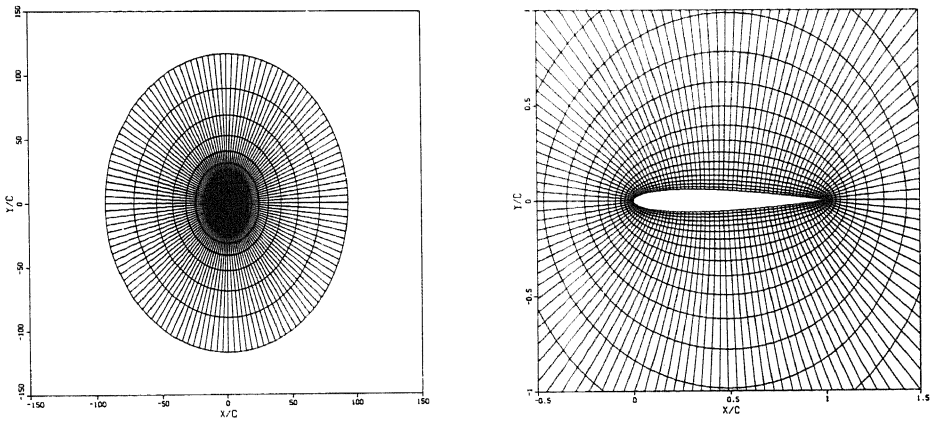

a. In full. b. In detail.

Fig. 5.10 : 128×32-grid.

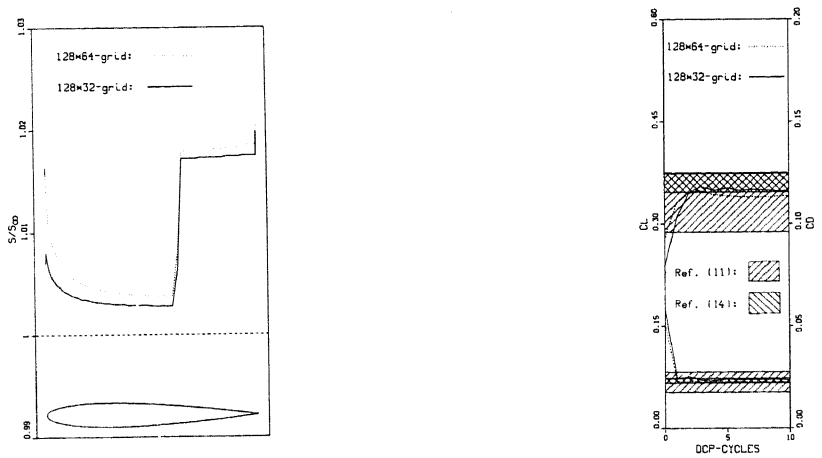

a. Upper surface entropy distributions. b. Convergence histories lift and drag coefficient.

Fig. 5.11 : Results 128×64- and 128×32-grid for NACA0012-airfoil at $M_\infty = 0.8$ and $\alpha = 1.25°$ (van Albada scheme).

In fig. 5.12-5.14 and in fig 5.16, we present comparisons for some other standard cases. As reference results for the lift and drag histories, we used all Euler results available from either [11] or [14]. As reference results for the distribution of some solution component, we only selected the best results from either [11] or [14].
Besides the NACA0012-airfoil, we also considered the NLR7301-airfoil.

For the NACA0012-airfoil, we considered as extra test cases: (i) $M_\infty = 0.63$, $\alpha = 2°$ (subcritical flow), (ii) $M_\infty = 0.85$, $\alpha = 1°$ (transonic flow with upper shock, lower shock and slip line), and (iii) $M_\infty = 1.2$, $\alpha = 7°$ (supersonic flow with detached bow shock, oblique tail shock and slip line). For all three cases, we used as finest grid: the 128×32-grid shown in fig. 5.10, and as DCP-strategy: 10 DCP-cycles with 1 FAS-cycle per DCP-cycle. As projection scheme for the subcritical test case, we used the upwind biased, the superbox as well as the van Albada scheme. For the transonic and supersonic test case, we only used the van Albada scheme.

Remarkable for the subcritical test case is the excellent agreement between the surface pressure distributions of the three second order schemes (fig. 5.12a). The agreement between our results and the reference results [11] is good. Very good is the drag yielded by the upwind biased and superbox scheme (fig. 5.12b). Both closely approach the exact zero-drag.

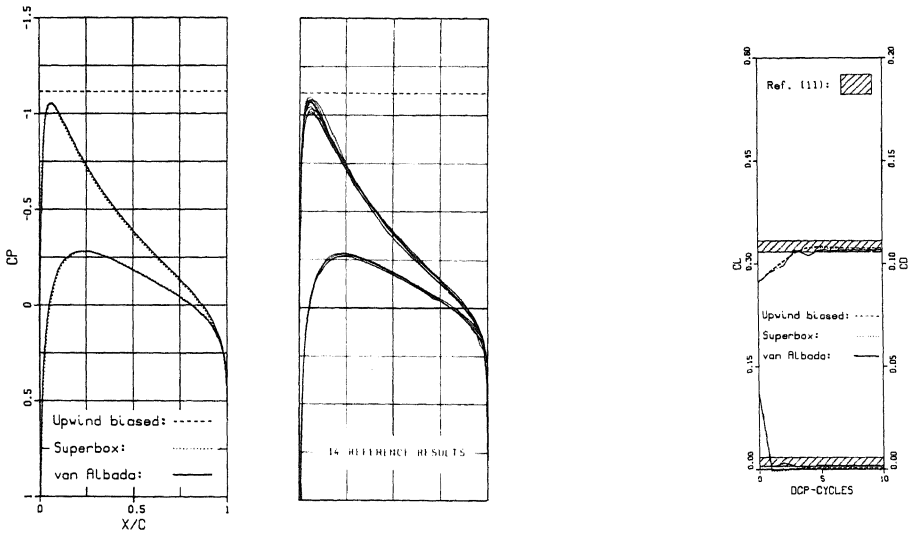

a. Surface pressure distributions; present results (left) and reference results (right).

b. Convergence histories lift and drag coefficient.

Fig. 5.12 : Results for NACA0012-airfoil at $M_\infty = 0.63$ and $\alpha = 2°$.

For the transonic test case, we compare our solution with those of SCHMIDT & JAMESON [14] and SALAS & SOUTH [14]. As grid, they used an O-type grid of 320×64 respectively 192×39. Although no evidence can be given that they both needed such a fine grid, it can be seen that we can use a significantly coarser grid. Our lift and drag agree well with theirs. (Schmidt & Jameson found: $c_l = 0.3472$, $c_d = 0.0557$ and Salas & South found: $c_l = 0.3584$, $c_d = 0.0580$, whereas we found: $c_l = 0.3565$, $c_d = 0.0582$). Further, all three discontinuities occurring in the flow are captured equally well in our results and the reference results (fig. 5.13a and 5.13c). Our entropy distribution (fig. 5.13d, no comparable results available) shows furthermore a very modest entropy error (0.002) just upstream of the foot of both shock waves. (The smearing of discontinuities in radial direction (fig. 5.13c and 5.13d) is only due to the grid enlargement in this direction.)

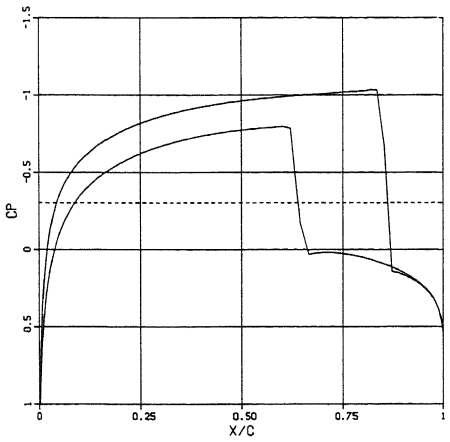

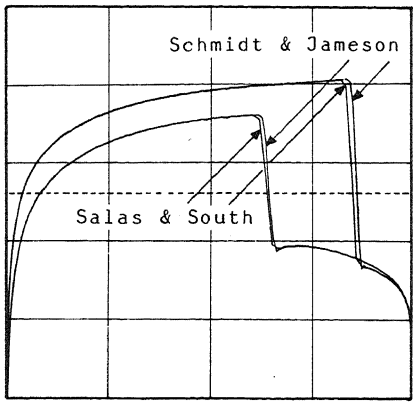

a. Surface pressure distributions; present result (left) and reference results (right).

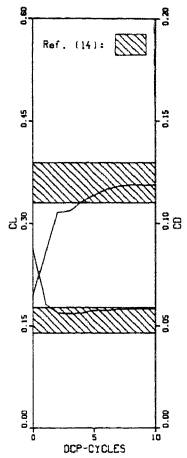

b. Convergence history lift and drag coefficient.

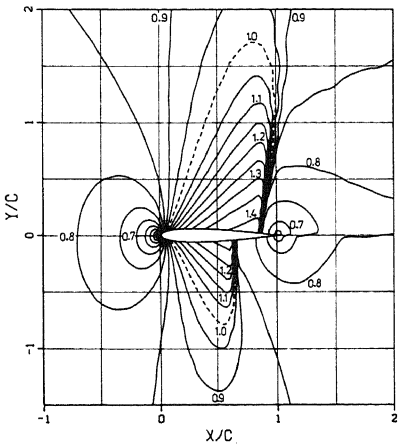

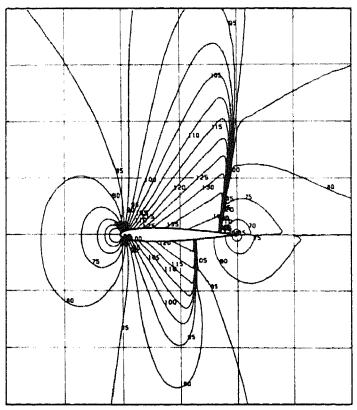

c. Mach number distributions; present result (left) and result Schmidt & Jameson (right).

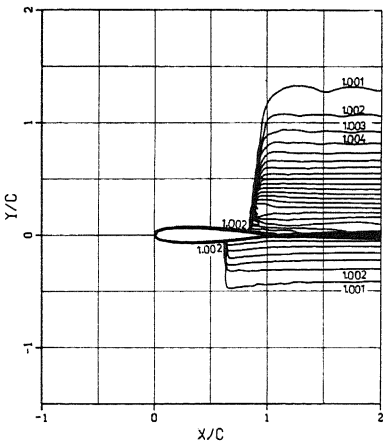

d. Present entropy distribution (s/s_∞).

Fig. 5.13 : Results for NACA0012-airfoil at $M_\infty = 0.85$ and $\alpha = 1°$ (van Albada scheme).

For the supersonic test case, we compare our solution with those of SCHMIDT & JAMESON [14] and VEUILLOT & VUILLOT [14]. As grid, they used a 320×64 O-type grid and a 201×55 C-type grid respectively. As lift and drag, they found: $c_l = 0.5138$, $c_d = 0.1538$ respectively $c_l = 0.5280$, $c_d = 0.1530$, whereas we found: $c_l = 0.5237$, $c_d = 0.1551$. Except for a slight difference in drag and upstream location of the bow shock (fig. 5.14c), the agreement between our results and the reference results is very good. Our entropy distribution (fig. 5.14d) shows a very modest entropy error (0.002) just upstream of the airfoil's tail. The same conclusion holds as for the previous test case: with an unadapted and relatively coarse grid, a good solution is obtained.

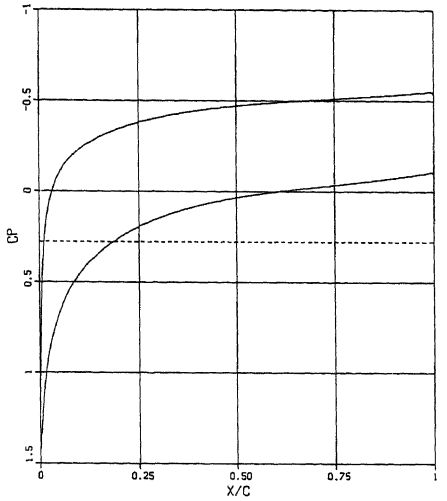

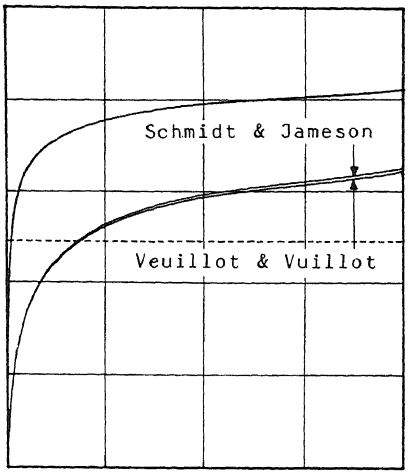

a. Surface pressure distributions; present result (left) and reference results (right).

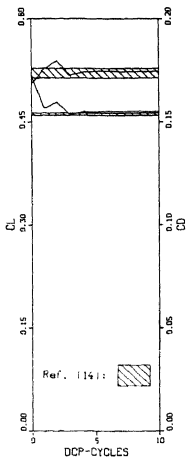

b. Convergence history lift and drag coefficient.

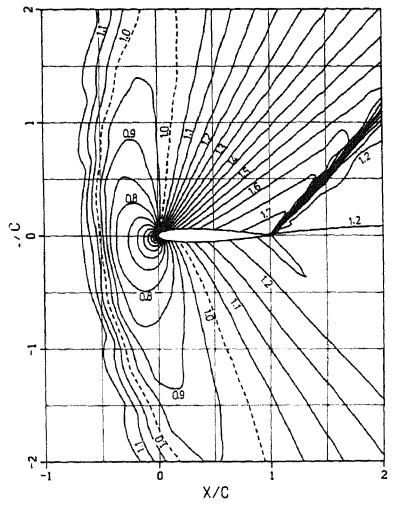

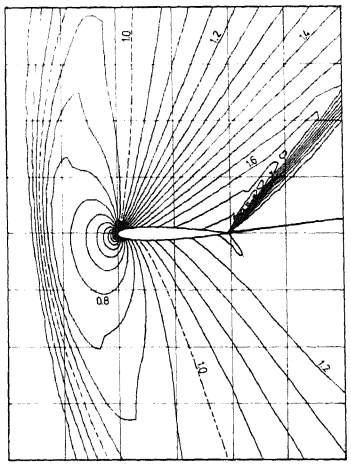

c. Mach number distributions; present result (left) and result Veuillot & Vuillot (right).

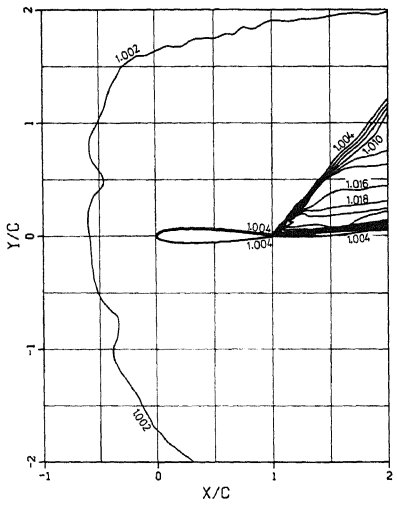

d. Present entropy distribution (s/s_∞).

Fig. 5.14 : Results for NACA0012-airfoil at $M_\infty = 1.2$ and $\alpha = 7°$ (van Albada scheme).

For the NLR7301-airfoil, we computed the flow at its design conditions: $M_\infty = 0.721$, $\alpha = -0.194°$ (supercritical shock-free flow). As projection scheme, we used the superbox scheme and as finest grid a 128×32-grid similar to the one used for the NACA0012-airfoil (fig. 5.15a). As DCP-strategy, we used again 10 DCP-cycles with 1 FAS-cycle per DCP-cycle. The exact solution, as computed by BOERSTOEL & HUIZING [2], could not be reproduced. The potential flow broke down in the neighbourhood of where the sonic line should fence off the most downstream part of the supersonic zone (fig. 5.16a and 5.16c). Computations with other projection schemes as well as computations with the

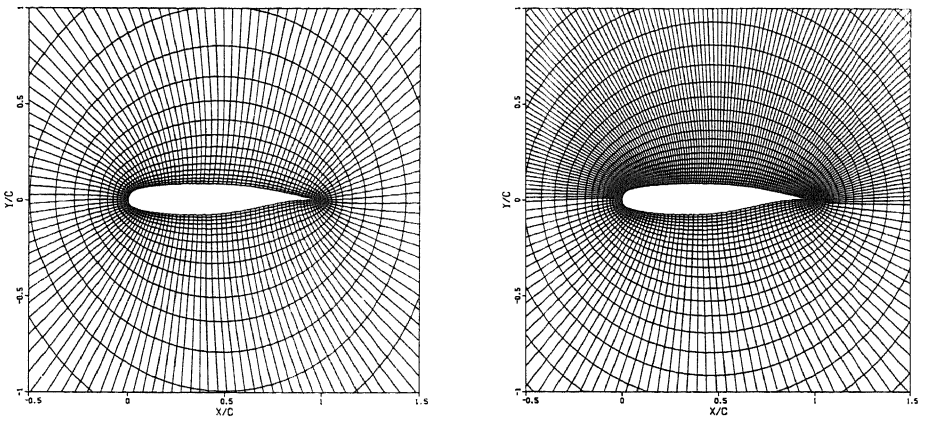

a. 128×32-grid. b. 192×48-grid.

Fig. 5.15 : Grids NLR7301-airfoil, in detail.

Korn1-airfoil at its design conditions, showed a similar break-down. We suspect that the cause of the break-down is an accumulation of discretization errors in the most downstream part of the supersonic zone. This accumulation can be explained with the mechanism of Mach lines emanating from the airfoil along the entire supersonic zone, reflecting at the sonic line, and finally focussing in the most downstream part of the supersonic zone. Yet, with an adapted grid as shown in fig. 5.15b, we did not obtain significant improvements. Concerning the reference results [14], it is noticed that most of them show some sort of break-down. Further, it is remarkable that SCHMIDT & JAMESON [14], who most closely approached the exact solution (fig. 5.16a), also used the finest grid (322×66 *O*-type). Given the good agreement for the previous test cases, between our results and those of Schmidt & Jameson it seems that if no elegant means of improvement can be found, strong overall grid refinement may still be used.

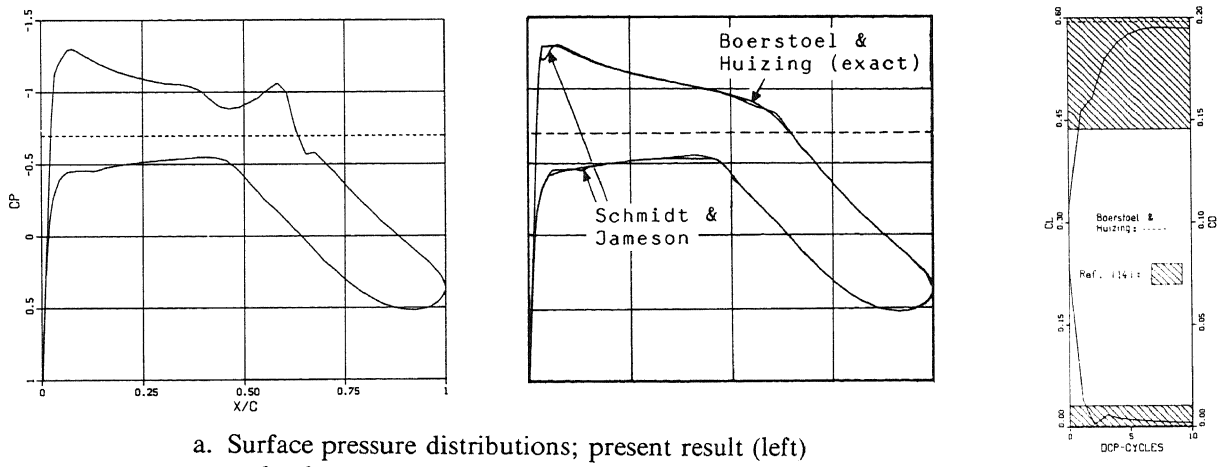

a. Surface pressure distributions; present result (left) and reference results (right).

b. Convergence history lift and drag coefficient.

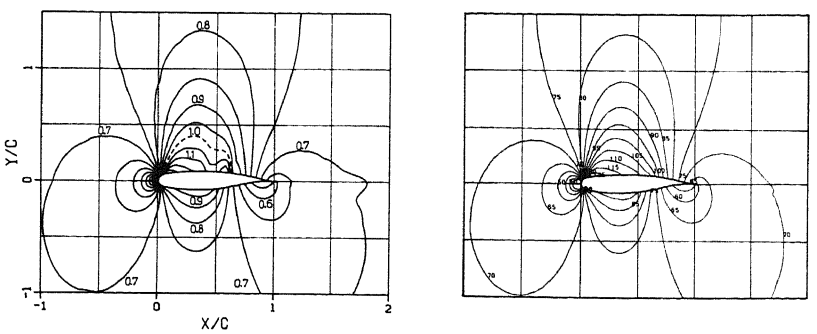

c. Mach number distributions; present result (left) and result Schmidt & Jameson (right).

Fig. 5.16 : Results for NLR7301-airfoil at $M_\infty = 0.721$ and $\alpha = -0.194°$ (superbox scheme).

For the airfoil flows computed on the 128×32-grid, we needed on an average 5 DCP-cycles to drive the lift coefficient to within $\frac{1}{2}\%$ of its final value. On the CDC Cyber 205 (single pipe version), this took us $\sim$ 100 sec (i.e. $\sim$ 25 msec per volume) in scalar mode, and $\sim$ 50 sec in vector mode. In scalar mode, we obtained the same computational rate per volume for both coarser and finer grids. The convergence rates of both FAS (inner iteration) and DCP (outer iteration) appear to be independent of the number of volumes on the finest grid (grid-independent).

We did not extensively tune our code for use on vector computers since we did not expect significant accelerations by vectorization. However, for large scale computations, where all data cannot be kept in core, the small number of iteration cycles required (5 DCP-cycles on an average) results in a small number of out-of-core data transports. For most Euler codes this is significantly more. Since IO-times rather than CPU-times may be the hampering factor in large scale computations on vector computers, we consider this feature as another advantage of the multigrid method used.

6. Conclusions

To compute airfoil flows, we considered five second order accurate projection schemes, in combination with defect correction iteration and a multigrid solution procedure.

Concerning the projection schemes, the central scheme was found to be unsuitable for the computation of airfoil flows with shock, whereas the upwind scheme was found to be unsuitable for any blunt-nosed airfoil flow. The three remaining schemes (the upwind biased, superbox and van Albada scheme) yield solutions of exactly the same good quality for subcritical flows. For flows with shock, the upwind biased and superbox scheme yield solutions with a too large under- and overshoot at the shock, but with a good quality in the smooth flow parts. For these flows, the van Albada scheme yields solutions with hardly any spurious non-monotonicity, solutions which are of good quality in both the smooth and non-smooth flow parts.

For the multigrid computation of airfoil flows with the steady Euler equations, DCP is found to be an efficient solution method for stable second order discretizations. It appeared that it is sufficient to perform only a few DCP-cycles (5 on an average), with only 1 FAS-cycle per DCP-cycle. Given the grid-independency of both FAS and DCP, an extension to 3-D seems to be feasible.

Comparison with the results of other investigators shows that for flows with discontinuities, we obtain solutions of the same good quality with a finest grid which may be twice as coarse (in both directions).

An important property of the present computational method is that it is parameter-free: it needs no tuning of parameters.

Acknowledgements

The author would like to thank P.W. Hemker for his valuable suggestions, J.W. Boerstoel and A. Kassies for their kind making of grids with NLR-software, and J.J. Rusch for his implementation of contour-plotting software.

This work was supported by the Netherlands Technology Foundation (STW).

7. References

[1] van Albada, G.D., van Leer, B., Roberts, W.W.: *A comparative study of computational methods in cosmic gasdynamics.* Astron. Astrophys. 108, 76-84 (1982).

[2] Boerstoel, J.W., Huizing, G.H.: *Transonic shock-free aerofoil designed by analytic hodograph methods.* AIAA paper 74-539 (1974).

[3] Böhmer, K., Hemker, P.W., Stetter, H.: *The defect correction approach.* Computing, Suppl. 5, 1-32 (1984).

[4] Eriksson, L.E., Rizzi, A.: *Computer-aided analysis of the convergence to steady state of discrete approximations to the Euler equations.* J. Comp. Phys. 57, 90-128 (1985).

[5] Hackbusch, W.: *Multigrid methods and applications.* Springer Series Comp. Mathematics 4, Springer Verlag, Berlin (1985).

[6] HEMKER, P.W.: *Defect correction and higher order schemes for the multigrid solution of the steady Euler equations.* Report NM-R8523, Centre for Mathematics and Computer Science, Amsterdam (1985). To appear in Proceedings Multigrid Conference, Cologne (1985).

[7] HEMKER, P.W., SPEKREIJSE, S.P.: *Multiple grid and Osher's scheme for the efficient solution of the steady Euler equations.* Report NM-R8507, Centre for Mathematics and Computer Science, Amsterdam (1985). To appear in Appl. Num. Math. (1986).

[8] KOREN, B.: *Euler flow solutions for a transonic windtunnel section.* Report NM-R8601, Centre for Mathematics and Computer Science, Amsterdam (1986). To be submitted to AIAA Journal in cooperation with C. Nebbeling.

[9] VAN LEER, B.: *Upwind-difference methods for aerodynamic problems governed by the Euler equations.* Lectures in Applied Mathematics 22, 327-336 (1985).

[10] OSHER, S.: *Numerical solution of singular perturbation problems and hyperbolic systems of conservation laws.* In: *Mathematical and numerical approaches to asymptotic problems in analysis.* Axelsson, O., Frank, L.S., van der Sluis, A. (eds.) , North Holland Publishing Company (1981).

[11] RIZZI, A., VIVIAND, H.: *Numerical methods for the computation of inviscid transonic flows with shock waves.* Vieweg Verlag (1981).

[12] SPEKREIJSE, S.P.: *Second order accurate upwind solutions of the 2-D steady Euler equations by the use of a defect correction method.* Report NM-R8520, Centre for Mathematics and Computer Science, Amsterdam (1985). To appear in Proceedings Multigrid Conference, Cologne (1985).

[13] SWEBY, P.K.: *High resolution schemes using flux limiters for hyperbolic conservation laws.* SIAM J. Num. Anal. 21, 995-1011 (1984).

[14] YOSHIHARA, H. et al: *Test cases for inviscid flow field methods.* AGARD advisory report 211 (1985).